Published online 10 December 2019 *Nucleic Acids Research, 2020, Vol. 48, No. 3* ***1097–1107***
doi: 10.1093/nar/gkz1125

Regioselective formation of RNA strands in the absence of magnesium ions

Sebastian Motsch, Peter Tremmel and Clemens Richert*

Institute of Organic Chemistry, University of Stuttgart, 70569 Stuttgart, Germany

Received October 08, 2019; Revised November 08, 2019; Editorial Decision November 14, 2019; Accepted November 18, 2019

ABSTRACT

The oligomerization of ribonucleotides can produce short RNA strands in the absence of enzymes. This reaction gives one of two regioisomeric phosphodiester linkages, a 2′,5′- or a 3′,5′-diester. The former, non-natural linkage is detrimental for duplex stability, and is known to form preferentially in oligomerizations occurring in homogeneous solution with preactivated nucleotides in the presence of magnesium cations. We have studied ribonucleotide oligomerization with *in situ* activation, using NMR as monitoring technique. Unexpectedly, the known preference for 2′,5′-linkages in the oligomerization of AMP was reversed in the absence of magnesium ions at slightly basic pH. Further, oligomerization was surprisingly efficient in the absence of Mg^{2+} salts, producing oligomers long enough for duplex formation. A quantitative systems chemistry analysis then revealed that the absence of magnesium ions favors the activation of nucleotides, and that the high concentration of active species can compensate for slower coupling. Further, organocatalytic intermediates can help to overcome the unfavorable regioselectivity of the magnesium-catalyzed reactions. Our findings allay concerns that RNA may have been difficult to form in the absence of enzymes. They also show that there is an efficient path to genetic material that does not require mineral surfaces or cations known to catalyze RNA hydrolysis.

INTRODUCTION

Oligoribonucleotides are believed to have been the first biopolymers that encoded genetic information (1). It is therefore important to know how RNA sequences form and undergo the reaction underlying replication in the absence of enzymes (2,3,4,5). One likely scenario is that ribonucleotides formed spontaneously from smaller precursors (6,7) were chemically activated, and then oligomerized to oligoribonucleotides (8). Starting from activated ribonucleoside phosphates, the chemical oligomerization reaction can produce two regioisomeric phosphodiesters: 2′-5′-linked diesters and 3′-5′-linked diesters, or 2′,5′-diesters/3′,5′-diesters, to be short (9). Isomerization of one regioisomer into the other can also occur, catalyzed by acid or small heterocycles (10), producing mixtures that are difficult to analyze with low-resolution techniques.

The 2′,5′-phosphodiester linkages mentioned above have a detrimental effect on the stability of RNA duplexes (11), although RNA structures with partial replacement of 3′,5′-linkages through 2′,5′-diesters can retain much of their functionality (12), and 2′,5′-linked sequences can act as templates for oligomerization of nucleotides (13). Further, a single 2′,5′-linkage in a duplex of otherwise 3′,5′-linked strands can lower hydrolytic stability up to 900-fold (14). As a consequence, regiospecificity of enzyme-free phosphodiester formation continues to be viewed as one of the central problems in the emergence of self-replicating RNA systems (15,16).

The regioisomeric composition of oligoribonucleotides has previously been studied by selective enzymatic hydrolysis, using nucleases that cleave 3′,5′-diesters and show little activity toward 2′,5′-diesters, followed by chromatographic analysis of the products (17). Using such a methodology, it was found that oligomerization of imidazolides in homogeneous solution predominantly gives 2′,5′-linkages (18,19). The formation of 3′,5′-linked oligomers can be favored by adding montmorillonite clay, where the interlayers of the clay platelets act as template (20). Up to two thirds 3′,5′-regioisomers were found in such templated oligomerizations when the imidazolide of adenosine 5′-monophosphate (Im-AMP) was used as starting material (21), and high values were also reported with 4-dimethylaminopyridine (22) or 1-methyladenine as organic leaving groups in such heterogeneous reaction mixture (23). Pyrimidines perform more poorly than purine nucleotides in these template-directed reactions (24). Further, a requirement for preactivated nucleotides and very specific mineral surfaces (20) severely reduces the probability for RNA to form in a prebiotic scenario. Alternative oligomerization scenarios require high temperatures and drying (25), which is incompatible with enzyme-free copying, or a eutectic phase (26), which

*To whom correspondence should be addressed. Tel: +49 711 685 64311; Fax: +49 711/685 64321; Email: lehrstuhl-2@oc.uni-stuttgart.de

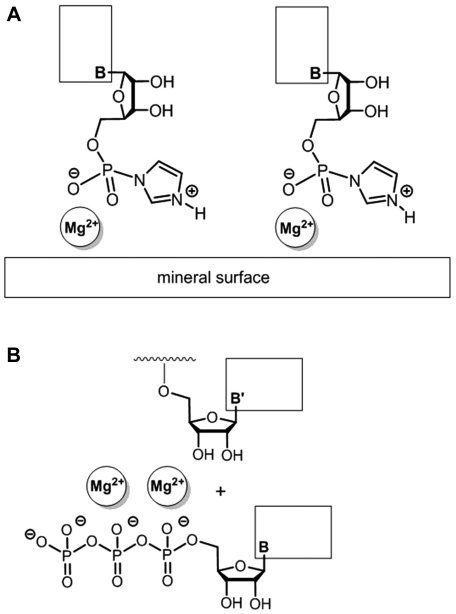

Figure 1. Magnesium ions in enzyme-free polymerization on montmorillonite minerals (**A**) and polymerase-catalyzed chain growth (**B**). The drawings are loosely based on structures shown in (33) and (29).

severely limits the prebiotic settings that can induce the desired process.

Efficient oligomerization of Im-AMP on clay minerals requires the presence of Mg^{2+} cations (27). Ferris and coworkers reported that "Na^{+}-montmorillonite alone did not produce products beyond dimer", but that assays with 75 mM magnesium chloride give oligomers up to decamers (28). Figure 1A shows a proposal for magnesium-mediated adsorption of the imidazolides of ribonucleotides on montmorillonite clay put forward by the same group (29). Magnesium ions are also found in the active site of polymerases and in RNA polymerase ribozymes. Both DNA and RNA polymerases bind their nucleoside triphosphate substrates with the help of two Mg^{2+} ions in their active site, as visualized schematically in Figure 1B. For ribozyme polymerases of class I, the key roles that magnesium ions play are believed to include screening of the negative charge of the phosphodiester backbone to allow for folding, coordination of functional groups in the active site, adjusting the pK_a of nucleophilic groups, and stabilizing transition states of the catalytic cycle (30).

Given the broad range of roles attributed to magnesium ions in reactions producing new backbone linkages of RNA, it seemed rather unlikely that phosphodiester formation would occur without magnesium in enzyme-free systems, which suffer from low reactivity to begin with. But, the presumed magnesium requirement complicates theories on how life first arose from simple molecules. It is unclear how much Mg^{2+} was available in the 'RNA world'. Lower concentrations of magnesium ions are believed to have existed in early oceans than today (31), and even today, 52 mM is a typical concentration in sea water, which is lower than the 75–200 mM concentrations typically employed in *in vitro* assays (29,32).

We have recently reported reaction conditions that lead to the formation of oligoribonucleotides from ribonucleotides in homogeneous aqueous medium, without preactivation and without mineral surfaces (34). The reaction solution contains a water-soluble condensation agent, a carbodiimide or cyanamide (35), and an organocatalyst, but it was unclear what the 2′/3′-regioselectivity of the reaction is. Further, it was not known what the active species are that drive the formation of phosphodiesters because activation occurs in the reaction solution. This prompted us to study the oligomerization reactions in 'Condensation Buffer' by NMR spectroscopy in an attempt to determine the phosphodiester isomer composition and formation in real time. Here we show how enzyme-free oligomerizations can be monitored by NMR without a need for digestion or intervention (36). Using this method, we found that strand formation from nucleotides with *in situ* activation can be quite efficient in the absence of magnesium cations. Additionally, the regioselectivity is more favorable in terms of the natural 3′,5′-regioisomer in the absence than in the presence of the divalent cations. This helps to allay concerns that RNA strands may have been difficult to generate in an enzyme-free medium lacking specific minerals (37).

MATERIALS AND METHODS

General. Chemicals and dry solvents were purchased from commercial suppliers and used without further purification. Adenosine 5′-monophosphate (AMP, free acid) was purchased from Carbosynth Ltd. (Berkshire, UK), cytidine 5′-monophosphate (CMP, disodium salt) from Sigma Aldrich (Deisenhofen, Germany), uridine 5′-monophosphate (UMP, disodium salt) from Acros (Geel, Belgium), and guanosine 5′-monophosphate (GMP, disodium salt monohydrate) from TCI (Zwijndrecht, Belgium). Preactivated nucleotide 2-MeIm-AMP (38) was synthesized according to the published procedure. D_2O (99.90% deuterated) was purchased from Euriso-Top (Saint-Aubin, France). ***NMR spectroscopy***. NMR spectra were acquired on a Bruker Avance III HD spectrometer (proton resonance frequency 700.36 MHz, phosphorus frequency 283.5 MHz) or a Bruker Avance III HD-NanoBay spectrometer (proton resonance frequency 400.10 MHz, phosphorus frequency 162 MHz). ^{1}H-NMR spectra were measured in the presence of either 3-(trimethylsilyl)-1-propanesulfonic acid sodium salt or 3-(trimethylsilyl)-propionic-2,2,3,3,-d_4 acid sodium salt as an internal standard. ***MALDI-TOF MS***. MALDI-TOF mass spectra were acquired on a Bruker Microflex mass spectrometer (Bruker Daltonics, Bremen, Germany) in linear negative mode. A mixture of 2:1 (v:v) of a 2,4,6-trihydroxyacetophenone solution (0.2 M in ethanol) and a diammonium citrate solution (0.1 M in H_2O) were used as matrix and co-matrix, respectively. ***ESI-HRMS***. High resolution mass spectra were recorded on a micrOTOF-Q mass spectrometer (Bruker Daltonics, Bremen, Germany), either in negative or positive mode. ***Chromatography***. Purification of dinucleotides on cartridge used Sep-Pak Vac C18 3cc RP-cartridges or Sep-Pak Vac QMA 3cc IEX-cartridges (Waters, Milford, MA, USA). The C18 cartridges were rinsed with MeCN and aqueous triethylammonium acetate (TEAA) buffer solution (100

mM, pH 7.5) before applying the product solution; QMA-cartridges were washed with a solution of $(NH_4)_2CO_3$ in H_2O (5 mM, pH 8.0). Alternatively, anion-exchange chromatography was performed on Express-Ion DEAE cellulose from GE Healthcare (Buckinghamshire, UK). Details are given in the respective sections, below. ***HPLC***. Reversed-phase HPLC was performed on a Rainin Dynamax Model SD-300 HPLC, using an analytical Nucleosil 120-5 C18 column (250 × 4.6 mm) from Macherey-Nagel (Düren, Germany). A gradient of MeCN in triethylammonium acetate (TEAA) buffer (0.1 M, pH 7.5) with a flow of 1 ml/min was used with detection at $\lambda = 260$ nm. ***Solid-phase RNA synthesis***. Automated solid-phase synthesis was performed on an ABI Expedite 8909 DNA synthesizer (PerSeptive Biosystems, Framingham, USA) using the phosphoramidite method and slightly modified settings recommended by the manufacturer. Reagents for oligonucleotide synthesis included controlled-pore glass (cpg) loaded with the 3′-terminal ribonucleoside and 2′-TBDMS-protected phosphoramidites from Sigma Aldrich (Taufkirchen, Germany). The 3′-TBDMS-protected phosphoramidites were from ChemGenes (Wilmington, MA, USA). Finally, the 'chemical phosphorylation reagent' 2-[2-(4,4′-dimethoxytrityloxy)ethylsulfonyl]ethyl-(2-cyanoethyl)-(*N*,*N*-diisopropyl) phosphoramidite was synthesized in-house following a known procedure (39).

Synthesis of reference compounds

Dinucleotides. The following protocol describes the synthesis of **pGG** and is representative for all dinucleotides. Solid-phase synthesis started from cpg loaded with the guanosine nucleoside (80 mg, 2 μmol). The first coupling cycle was performed with the 3′-TBDMS protected guanosine building block and the second with 'chemical phosphorylation reagent'. Afterwards, the solid support was treated with aqueous ammonia/aqueous methylamine (1:1 v/v; 'AMA') solution (750 μl) for 15 min at 55°C. The supernatant was harvested, and the residue was washed with H_2O (3 × 500 μl). The combined aqueous solutions were freed from ammonia and methylamine with a nitrogen stream directed onto the surface of the solution and then lyophilized to dryness. The resulting solid was dissolved in TEAA buffer (1 ml, 100 mM) and loaded onto a C18 SepPac cartridge (500 mg). The TBDMS-protected dinucleotide was eluted with a gradient of MeCN in TEAA buffer (0–25% MeCN, in 5% steps, 5 ml each). Product-containing fractions were collected and lyophilized. The resulting solid was dissolved in triethylamine trihydrofluoride (750 μl) and the solution was allowed to shake for 5 h at room temperature. Then, methoxytrimethylsilane (5 ml) was added, and the mixture was shaken vigorously for 5 min. The suspension was centrifuged for 5 min, and the supernatant was decanted off. The pellet was dissolved in TEAA buffer (1 ml, 100 mM) and again loaded onto a C18 SepPac cartridge (500 mg). After rinsing with TEAA buffer (4.5 ml, 100 mM) the deprotected dinucleotide was eluted with H_2O (10 ml). Fractions containing the fully deprotected dinucleotide were pooled and dried *in vacuo*.

5′-Pyrophosphate-capped dinucleotides. The following protocol is for **AppAA** and is representative. A sample of **pAA** (triethylammonium salt, 0.88 mg, 1.0 μmol, 1.0 equiv) was dissolved in a buffer solution (15 μl) containing HEPES (1.8 mg, 7.5 μmol, 500 mM) and $MgCl_2$ (0.11 mg, 1.2 μmol, 80 mM) at pH 7.5. Then, 2-MeIm-AMP (2.64 mg, 6.1 μmol, 6.1 equiv, 510 mM) was added, and the reaction mixture was incubated at 40°C. After 16 h, additional 2-MeIm-AMP (1.02 mg, 2.4 μmol, 2.4 equiv) was added, and the reaction was allowed to proceed for 5 h at 40°C. Then, the product was pre-purified by anion exchange chromatography (DEAE cellulose), using a step-gradient of ammonium bicarbonate in H_2O (0–200 mM bicarbonate, 20 mM steps, 6 ml each). Products were detected in fractions with 140–200 mM bicarbonate. The fractions were collected, freeze-dried, and the product was re-purified by HPLC (C18, MeCN gradient in 100 mM aqueous TEAA buffer, 0% to 15% in 45 min, $t_R = 31$ min). Excess TEAA buffer was removed via C18 SepPac cartridge. For this, the product was dissolved in TEAA buffer (1 ml, 100 mM) and loaded on the cartridge (500 mg). After washing with water (6 ml), the product was eluted with a solution of MeCN in H_2O (6 ml, 5% MeCN). The solvents were removed by lyophilization to obtain a colorless powder.

Dipeptido-dinucleotides. This protocol is for **GlyGlyAA** and is representative. The triethylammonium salt of dinucleotide **pAA** (0.22 mg, 250 nmol, 1.0 equiv) was dissolved in a freshly prepared solution (D_2O, 100 μl) containing EDC hydrochloride (15.3 mg, 80 μmol, 320 equiv, 800 mM) and DMAP (1.80 mg, 15 μmol, 60 equiv, 150 mM) at pH 8.0, uncorrected for deuterium effect. After 3 h at 22°C, the reaction mixture was added to a solution of $NaClO_4$ in acetone/Et_2O (3 ml, 0.1 M, 1:1 v/v) at 0°C. After vigorous shaking, the suspension was kept in an ice bath for 10 min. Then, the suspension was centrifuged for 5 min, and the supernatant was decanted. The pellet thus obtained was washed with Et_2O (1 ml) twice, and then dried at 15 mbar in a desiccator. The pellet was dissolved in a solution of glycylglycine (7.92 mg, 60 μmol, 240 equiv, 300 mM) in D_2O (200 μl) at pH 7.5. The reaction mixture was incubated for 3 h at 22°C. Afterwards, the solution was diluted with TEAA buffer (1 ml, 100 mM) and loaded onto a C18 SepPac cartridge (500 mg). The product was eluted with a step gradient of MeCN in 100 mM TEAA buffer (0–14%, 2%-steps, 2 ml each). Product-containing fractions (6–8% MeCN) were pooled and lyophilized. Residual TEAA buffer was removed by adsorbing the product on a C18 SepPac cartridge, followed by elution with water/acetonitrile and lyophilization, as described in the protocol for 5′-pyrophosphate-capped dinucleotides.

Oligomerization assays

The following protocol is for the oligomerization of AMP and is representative for the NMP oligomerization assays. To AMP (free acid, 34.7 mg, 100 μmol), 1-ethylimidazole (7.2 μl, 75 μmol), and (where necessary) $MgCl_2$ (0–3.8 mg, 0–40 μmol) was added D_2O (450 μl), followed by addition of NaOH solution (up to 10 μl, 10 M) to aid dissolution,

vortexing, and adjusting the pH to 7.5, again using 10 M NaOH solution in D_2O. The resulting solution was cooled to 0°C. Then, EDC hydrochloride (76.7 mg, 400 μmol) was added to obtain a volume of 500 μl of a solution containing AMP (0.2 M), EDC (0.8 M), 1-EtIm (0.15 M) with or without $MgCl_2$ (0–80 mM). The reaction was allowed to proceed at 0°C for 24 h. The mixture was then transferred to an NMR tube and analyzed by ^{31}P-NMR (162 MHz) at room temperature. Reaction mixtures containing 80 mM $MgCl_2$ were diluted by adding a solution of EDTA (15.0 mg, 40 μmol) in D_2O (250 μl) at pH 8.0, before NMR measurements were performed.

Kinetics of magnesium-free oligomerization of AMP

A solution of MOPS buffer (0.4 ml) containing MOPS (105 mg, 0.5 mmol, 1.25 M) and 1-ethylimidazole (7.2 μl, 75 μmol, 0.187 M) at pH 7.5 was treated with AMP (35 mg, 0.1 mmol). The pH was adjusted to 7.5 using NaOH solution (10 M). Then, D_2O (50 μl) was added and the solution was cooled to 0°C, followed by addition of EDC hydrochloride (77 mg, 0.4 mmol) to give the following final concentrations: AMP (0.2 M), EDC (0.8 M), MOPS (1 M) and 1-ethylimidazole (0.15 M) in 0.5 ml solution. After the addition of EDC, 0.5 ml of the ice-cooled reaction mixture was placed in an NMR tube, and immediately transferred to a 700 MHz NMR spectrometer set to 1°C probe temperature. The first spectrum was recorded 30 min after addition of EDC, followed by 1 h intervals. At each time point, a ^{1}H-NMR spectrum was acquired, followed by a ^{31}P-NMR spectrum with a recycle delay of 10 s. The concentrations of AMP, and of the sum of AppA, and EI-AMP were determined from signals in ^{31}P-NMR spectra by integration. Concentrations of EI-EDC, EDC, and EDU, as well as the ratio of EI-AMP to AppA were extracted from integration of ^{1}H-NMR spectra. For EDC and the EDC-derived species, triplets of the methyl groups of the ethyl chains were used for integration because they are well separated from other signals in the spectrum.

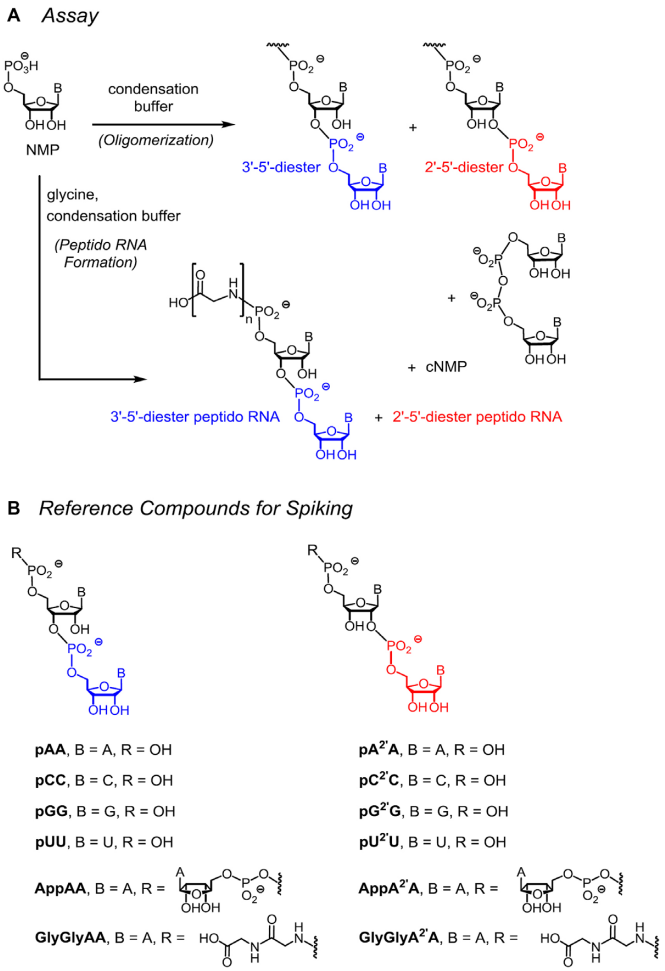

Scheme 1. Formation of 3′,5′- and 2′,5′-diesters in enzyme-free oligomerization of ribonucleotides or peptido RNA formation in the presence of an amino acid.

RESULTS

Assays

Figure 1A shows the ribonucleotide oligomerizations that were to be studied for the regioselectivity of phosphodiester formation. They include assays in the presence of glycine. In the former case, oligoribonucleotide strands are formed, together with pyrophosphates and cyclic species (34). The latter assays were expected to give peptido RNAs as the main product (40,42). In peptido RNAs, a peptide chain is *N*-terminally linked to the 5′-phosphate of a ribonucleotide or oligoribonucleotide. Peptido RNAs were recently found in aqueous condensation buffer containing water-soluble carbodiimide EDC and 1-ethylimidazole as organocatalyst (40,41). Much like the oligoribonucleotides that form in the untemplated oligomerizations (34,42), peptido RNAs were expected to contain significant quantities of 2′,5′-phosphodiester linkages. The formation of phosphodiesters and phosphoramidates, and diesters of cyclic mono- or dinucleotides, was to be detected by NMR.

We chose NMR as analytical tool because enzyme-based methodologies have drawbacks. Among them are that the substrate specificity of nucleases depends on the sequence to be digested (43), and that digestion destroys the newly formed material. Nuclease digestion leads to the loss of sequence information, makes the method unsuitable for *in situ* monitoring, and complicates kinetic studies. Further, substrates that contain non-nucleosidic substituents and condensation agents may affect the ability of nucleases to digest phosphodiesters reliably. Among the substituents that may have such an effect are covalently linked peptides, as in peptido RNAs formed in reactions of amino acids and ribonucleotides. The literature on NMR of 2′,5′-linked oligonucleotides (44–48) suggested that NMR might by suitable for detecting the regioisomeric composition of new formed strands. But, to the best of our knowledge, there are no literature reports on monitoring template-free oligomerization of ribonucleotides by NMR (Scheme 1).

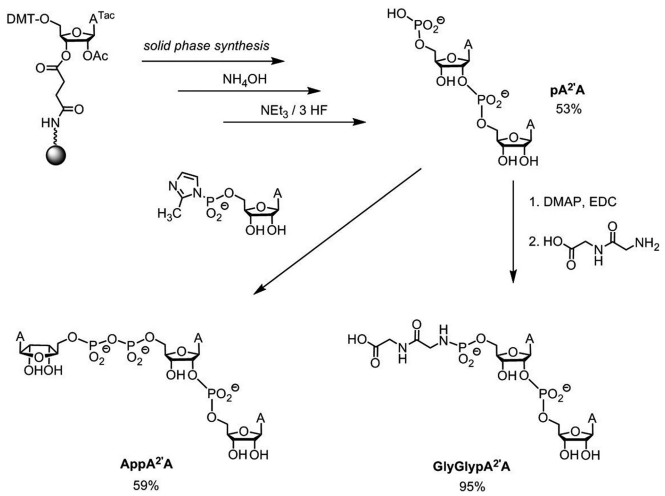

Scheme 2. Synthetic approaches employed to synthesize reference compounds with 5′-caps, shown for two representative compounds, 5′-pyrophosphate-capped dinucleotide **AppA$^{2'}$A** and dipeptido-dinucleotide **GlyGlyA$^{2'}$A**. Chain extension was by automatic RNA synthesis, subsequent coupling to dipeptido dinucleotides or pyrophosphate-capped dinucleotides was by solution phase syntheses. See the Supplementary Information for the syntheses of other reference compounds, protocols and analytical data. The percentages given are chemical yields.

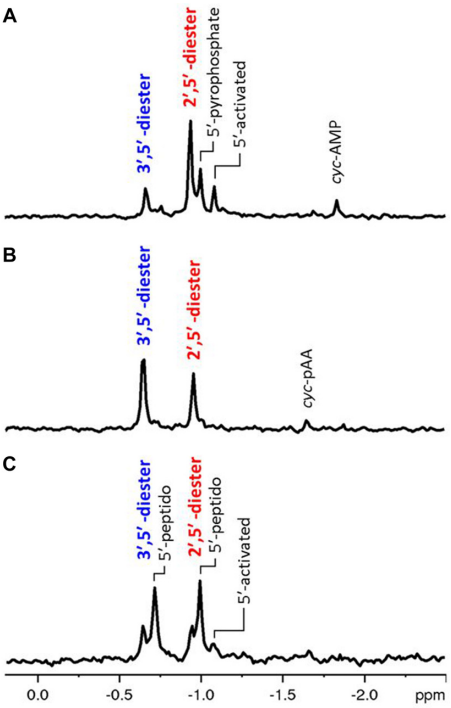

Figure 2. Phosphodiester region of ^{31}P-NMR spectra (162 MHz, D_2O) from AMP oligomerization assays in the presence or absence of $MgCl_2$ and glycine at 0°C. (**A**) 0.2 M AMP, 0.08 M $MgCl_2$, pH 7.5, after 24 h and addition of EDTA; (**B**) 0.2 M AMP without $MgCl_2$, pH 8.5, after 24 h; (**C**) AMP and glycine, 0.2 M each, without $MgCl_2$, pH 7.5 after 48 h.

Synthesis of reference compounds

The condensation buffer contains a high concentration of solutes that affect chemical shifts. Further, pyrophosphate formation is a fast reaction, so that phosphodiester products are often 5′-capped by a pyrophosphate-linked nucleotide, even when early time points are analyzed. Hence, we synthesized the reference compounds shown in Figure 1B to verify our peak assignments by spiking. The reference compounds were dinucleotides with 2′,5′- or 3′,5′-diester backbone, with or without a 5′-pyrophosphate cap or dipeptido substituent. The 2′,5′-linked species are given as pN$^{2'}$N in the short-hand used, where N are the nucleobases. Dinucleotides were synthesized on solid support using 2′-TBDMS or 3′-TBDMS-protected phosphoramidites and 'chemical phosphorylation agent' (39) for the final coupling cycle. In the case of the diadenylates **pAA** and **pA$^{2'}$A**, the dinucleotides were also converted to the dipeptido or pyrophosphate-linked species that are shown in the lower part of Figure 1B. The coupling of the dipeptide used the dimethylaminopyridinium dinucleotide as activated species, whereas the pyrophosphates were prepared by reacting the dinucleotides with the 2-methylimidazolide of AMP (Scheme 2). Further details and analytical data are given in the Supplementary Information (Supplementary Scheme S1 and Supplementary Figures S1–S16).

Regioselectivity of phosphodiester formation

Spectra of mixtures of regioisomers showed ^{31}P-signals of 2′,5′-diesters at higher field than those of the 3′,5′-diesters. This was also true for mixtures containing the components of condensation buffer, as confirmed by spiking (Supplementary Figures S22 and S23, SI). Figure 2A shows a representative ^{31}P-NMR spectrum from the oligomerization of AMP in a HEPES-free version (40) of general condensation buffer (0.8 M EDC, 0.15 M 1-EtIm, 0.08 M $MgCl_2$, pH 7.5). At high magnesium concentrations, narrow linewidths were obtained when EDTA was added prior to acquiring spectra, but this step could be avoided in later versions (*vide infra*). The 2′,5′-diesters gave more intense peaks than the 3′,5′-counterparts. This was true for the free dinucleotides as well as 5′-pyrophosphate and 5′-activated (imidazolium) species that forms from the initial isourea upon the addition of the nucleotide to the carbodiimide (35). Integration of the regions for either type of diester gave a ratio of 3′,5′- to 2′,5′-diesters of approx. 1:4. Analogous assays were performed with CMP, GMP and UMP, which gave regioisomeric ratios ranging from 10:90 to 26:74 (Table 1). Representative ^{31}P-NMR spectra are shown in the Supplementary Information (Supplementary Figures S17–S21).

Pyrophosphate formation is strongly dependent on the concentration of divalent cations. To favor phosphodiester formation, we lowered the Mg^{2+} concentration step-wise in the AMP assays. This did reduce the amount of pyrophosphates from 24% to 6% (Supplementary Table S1, SI), but, unexpectedly, it also changed the regioselectivity of diester formation. In the absence of divalent cations, the 3′,5′-diesters were found to almost the same extent as the 2′,5′-esters (48:52, entry 10 of Table 1). A shift toward 3′,5′-esters was found for all four bases (A/C/G/U). Even more surprisingly, the rate of formation of phosphodiesters did not collapse in the absence of $MgCl_2$ for any of the four nucleobases. For AMP, the diester concentration in the mixture

Table 1. Product distribution and regioselectivity of oligomerization of ribonucleotides, as determined by ^{31}P-NMR spectroscopy after 24 h[a]

NMP	$MgCl_2$ [mM]	Initial pH[b]	Pyrophosphates [%]	Phosphodiesters [%]	Ratio 3′,5′: 2′,5′
UMP	80	7.5	10.4	3.1	26:74
UMP	-	7.5	3.3	2.0	34:66
CMP	80	7.5	9.7	5.4	23:77
CMP	-	7.5	4.0	3.4	33:67
GMP[c]	80	7.5	34	7.7	10:90
GMP	-	7.5	12.3	2.2	19:81
AMP	80	7.5	24.3	4.7	19:81
AMP	40	7.5	18.3	4.1	27:73
AMP	20	7.5	14.2	4.5	37:63
AMP	-	7.5	6.2	5.9	48:52
AMP	-	6.5	13.1	7.9	38:62
AMP	-	7.0	10.2	7.5	40:60
AMP	-	8.0	3.0	4.1	53:47
AMP		8.5	1.4	2.3	60:40
2-MeIm-AMP[d]	-	7.5	7.5	0.6	28:72
AMP+Gly[e]	80	7.5	11.1	0.8	20:80
AMP+Gly[e]	-	7.5	5.3	2.8	48:52

[a]Conditions: EDC hydrochloride (800 mM), 1-EtIm (150 mM). D_2O, 0°C, 24 h.
[b]No buffer used, slight shift to basic pH over the course of the assay, mostly due to consumption of 5′-phosphates.
[c]20 mM GMP and 8-day reaction time due to low solubility in the presence of $MgCl_2$.
[d]2-MeIm-AMP (200 mM) in D_2O, pH 7.5, 0°C, after 24-day reaction time.
[e]Reaction time 2 days.

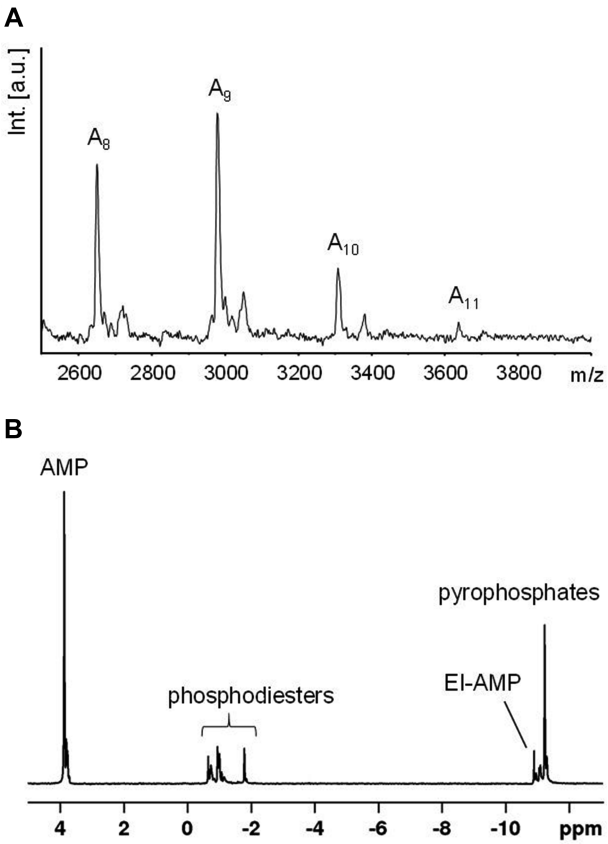

Figure 3. Oligomerization of AMP in the absence of Mg^{2+} and buffer salts at a starting pH of 7.0 and 7 d reaction time (0.2 M AMP, 0.8 M EDC, 0.15 M EtIm, D_2O, pH 7.0, 0°C). (**A**) MALDI–TOF-MS spectrum of a late fraction eluting from an anion exchange cartridge showing oligomers (see the Supplementary Information for conditions). (**B**) ^{31}P-NMR spectrum (162 MHz, D_2O) acquired after 7-day reaction time. Integration of the peaks in the phosphodiester region gave a value of 20.6%. See Table 2 for additional data obtained at the same reaction time.

Table 2. Longest detectable RNA chain in AMP oligomerization after 7-day reaction time, as observed by MALDI–TOF MS

$MgCl_2$ [mM]	HEPES [mM]	Initial pH	Phosphodiester (non-cyclic) [%][a]	Longest detectable chain[b]
80	500	7.5	10.7	A_{10}
-	-	6.5	21.1	A_{11}
-	-	7.0	20.6	A_{11}
-	-	7.5	17.3	A_9
-	-	8.0	12.6	A_8
-	-	8.5	6.6	A_7

[a]Determined by ^{31}P-NMR spectroscopy (162 MHz, D_2O).
[b]Determined by MALDI–TOF-MS after separation of the oligoadenylate mixture by anion exchange chromatography.

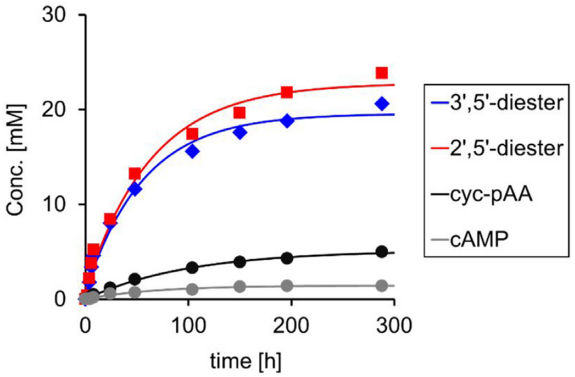

Figure 4. Kinetics of oligomerization and cyclization of AMP, as determined by ^{31}P-NMR spectroscopy. Symbols are experimental data points and lines are monoexponential fits. Conditions: 0.2 M AMP, 0.8 M EDC, 0.15 M 1-EtIm, pH 7.5, 0°C.

was even higher after 24 h than in the original, dication-rich medium (Table 1).

Next, we varied the pH value in the AMP oligomerization (Table 1, entries 11–14). Weakly basic conditions were

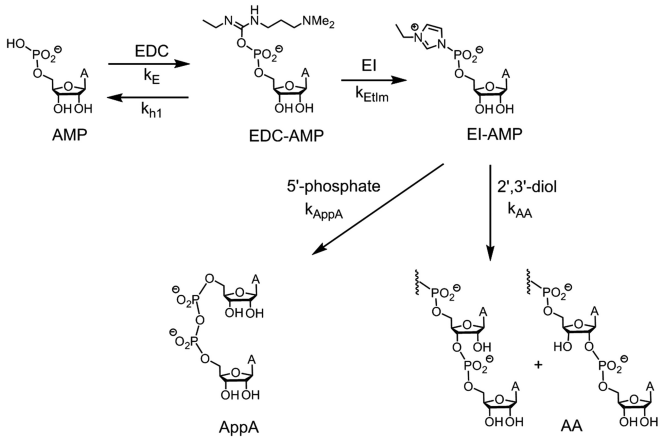

Figure 5. Reaction scheme showing intermediates of the EDC-induced oligomerization reaction in the presence of 1-ethylimidazole as organocatalyst. The short-hand used for rate constants (k) is shown next to each reaction arrow.

Table 3. Rate constants for steps involved in phosphodiester and pyrophosphate formation in the oligomerization of AMP in the presence and absence of $MgCl_2$[a]

Rate constant[b]	Order of reaction	Value of rate constant without $MgCl_2$	Value of rate constant with $MgCl_2$[c]
k_E	2nd	1.2 10^{-4} mM^{-1} h^{-1}	4.5 10^{-5} mM^{-1} h^{-1}
k_{EtIm}	2nd	0.5 mM^{-1} h^{-1}	0.5 mM^{-1} h^{-1}
k_{AppA}	2nd	0.9 10^{-4} mM^{-1} h^{-1}	8.3 10^{-4} mM^{-1} h^{-1}
k_{AA}	2nd	1.3 10^{-5} mM^{-1} h^{-1}	7.5 10^{-5} mM^{-1} h^{-1}

[a]Conditions: 0.8 M EDC, 0.15 M EI, no or 0.08 M $MgCl_2$, 1 M MOPS, H_2O/D_2O 9:1, pH 7.5, 0°C.
[b]See Figure 5 for reaction scheme.
[c]From (35).

found to favor 3′,5′-diesters. The highest selectivity toward the natural 3′,5′-regioisomer in the oligomerization of AMP (60:40) was obtained at pH 8.5 in the absence of dications. To the best of our knowledge, this is the first case of an untemplated enzyme-free oligomerization of a ribonucleotide in homogeneous aqueous solution that gives 3′,5′-phosphodiesters as the major regioisomer. Further, the reaction is largely unencumbered by pyrophosphates and cyclic byproducts, with the diesters as the dominant species (Figure 2B). When the pre-activated 2-methylimidazolide of AMP (2-MeIm-AMP) as the most established building block for oligomerization reactions was used in magnesium-free medium, less than 1% conversion to phosphodiesters was measured after more than three weeks reaction time. What little phosphodiester there was, had predominantly 2′,5′-linkages (ratio 72:28, Table 1). Further, pyrophosphates were formed to a much larger extent than phosphodiesters. So, the efficient and regioselective oligomerization under *in situ* activation conditions is not found for the pre-activated nucleotide.

Monitoring by NMR was also successful for reactions producing peptido RNAs, which are not the natural substrates of known enzymes. Figure 2C shows an example of a ^{31}P-NMR spectrum from an assay with equimolar amounts of glycine and AMP. A spectrum from an assay

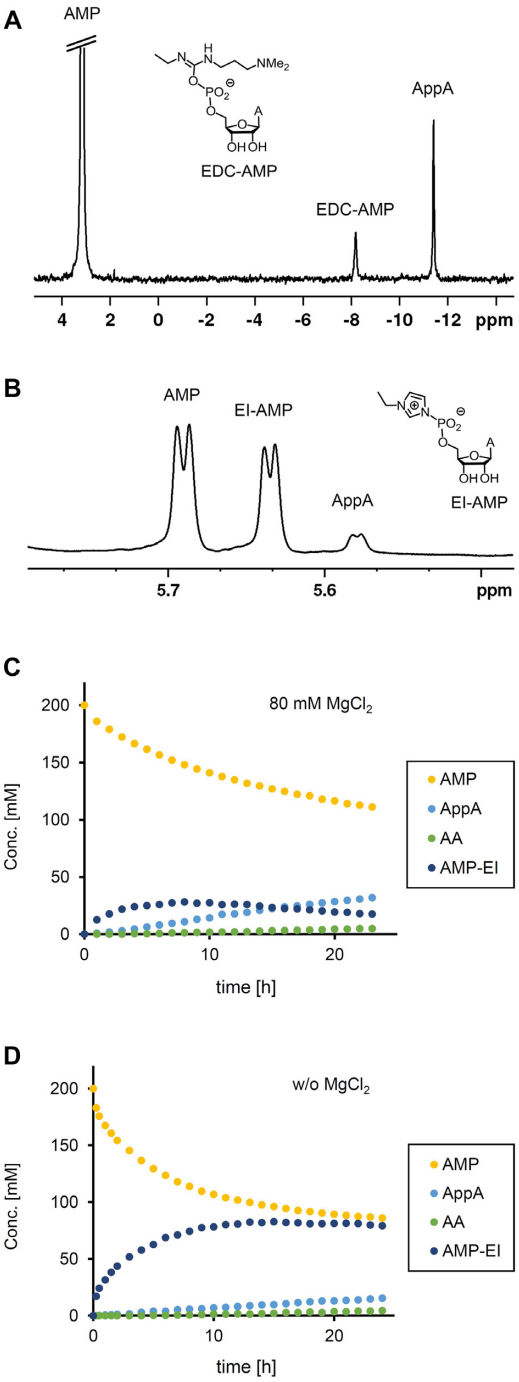

Figure 6. Build-up of active species in the oligomerization of AMP. (**A**) ^{31}P-NMR spectrum (283.5 MHz, H_2O/D_2O, 9:1) from oligomerization of AMP in the absence of 1-ethylimidazole after 12 h, showing a peak for the initial adduct of nucleotide and carbodiimide, the isourea EDC-AMP. Conditions: 0.8 M EDC, 1 M MOPS, H_2O/D_2O 9:1, pH 7.5, 0°C. (**B**) ^{1}H-NMR spectrum (700 MHz, H_2O/D_2O, 9:1) from oligomerization of AMP in the presence of 1-ethylimidazole (0.8 M EDC, 0.15 M EI, 1 M MOPS, H_2O/D_2O 9:1, pH 7.5, 0°C) after 12 h, with an intense peak for imidazolium nucleotide EI-AMP. (**C**) Kinetics of the conversion of AMP to EI-AMP, oligomers with phosphodiester linkages (AA), and pyrophosphates (AppA) in the presence of $MgCl_2$, as determined by NMR. Conditions: 0.8 M EDC, 0.15 M EI, 0.08 M $MgCl_2$, 0.5 M HEPES, H_2O/D_2O 9:1, pH 7.5, 0°C (**D**) Kinetics of the same reactions in the absence of $MgCl_2$; conditions: 0.8 M EDC, 0.15 M EI, 0.08 M $MgCl_2$, 1 M MOPS, H_2O/D_2O 9:1, pH 7.5, 0°C.

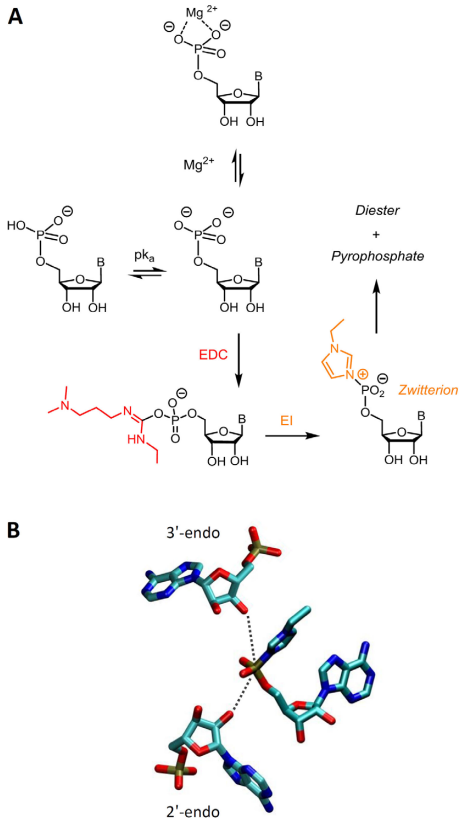

Figure 7. Activation and coupling in the presence of an organocatalyst. (**A**) Steps of the activation pathway with or without magnesium ions that form a chelate with the kinetically relevant dianion of AMP, and (**B**) Structure of ethylimidazolium-AMP (coordinates generated in Chem3D Pro 14.0) and two randomly oriented AMP molecules of different sugar pucker, 3′-endo (49) or 2′-endo (50) conformation, with possible nucleophilic lines of attack. The nucleophilically attacking nucleotide structures were generated using coordinates from X-ray crystal structures ADPOSM and ADPOSM01 in the CSD database. The structures were visualized in VMD. Trajectories of the competing nucleophilic attacks for the sterically less hindered hydroxy groups in pseudo-equatorial position are indicated by broken lines.

at 80 mM $MgCl_2$ is shown in Supplementary Figure S21 (SI). As expected, the peptido RNAs dominate over the neat oligoribonucleotides, but unreacted 5′-phosphate, and 5′-imidazolium phosphates were also detectable under our reaction conditions. Despite the very intense peaks for peptido species and the complex reaction mixture, the ratio of regioisomeric diesters could be determined, even on a 9.4 T spectrometer (400 MHz ^{1}H resonance frequency).

The screen underlying the data in Table 1 used analysis after a reaction time of 24 h, when the process of oligomerization is far from complete. We therefore analyzed representative assays after longer reaction times. First, we confirmed that the magnesium-free reaction conditions lead to chain lengths similar to those previously reported for oligomerization in conventional condensation buffer (40). Figure 3 shows spectra obtained after a reaction time of one week at pH 7.0. Oligoadenylates up to undecamers were readily detectable in the MALDI-TOF mass spectrum shown in Figure 3A, measured after fractionation by anion exchange cartridge treatment of the crude assay mixture. Further, Figure 3B shows a ^{31}P-NMR spectrum acquired after one week. The phosphodiesters among the ^{31}P signals were approx. 21% at this time point at pH 7. At pH 7.5, the integration value for diesters was 17.3%. This is more than observed in the presence of Mg^{2+} at this pH (Table 2), confirming that strand growth is superior to that in condensation buffer with 80 mM $MgCl_2$.

Next, we confirmed that there is no shift in regioselectivity over time, using our NMR-based method for *in situ* monitoring. Figure 4 shows kinetics for the oligomerization of AMP at pH 7.5. The lag phase expected for reactions with *in situ* activation is very brief, and either of the regioisomeric linkages is formed with at a similar rate. A simple monoexponential was found to fit the data surprisingly well, given that activation and coupling have to occur sequentially. Further, the cyclizations to cyclic monomer and dimer that accompanies chain growth gives similar kinetics, even though the stoichiometry of the underlying reactions is different. There is no detectable lag phase for the build-up of EI-AMP. This data suggests that among the activation processes, the first is rate-limiting. The hypothesis that the first activation step is rate limiting is also in agreement with the differences in the rate constants for the first and the second activation step (kE << kEtIm, Supplementary Table S1).

Systems chemistry analysis

We then proceeded to a detailed analysis of the reaction network to shed light on the molecular basis for the high-yielding oligomerization. We have recently reported a systems chemistry approach for reactions producing peptido RNAs in conventional condensation buffer (35). This approach relies on determining rate constants in a series of NMR-monitored assays of increasing complexity, and modeling the system in a set of coupled differential equations. The mathematical model allows one to track the fate of the reaction partners over time. In the present case, we were interested in determining which reaction steps are more efficient in the magnesium-free medium than in conventional condensation buffer. In order to avoid a pH shift that complicates the kinetic picture, we used MOPS buffer in the assays. Figure 5 shows steps of the reaction sequence underlying oligomerization and pyrophosphate formation, for which rate constants (k) were determined. Plots of kinetic data and the theoretical time-yield curves obtained from the model are shown in Supplementary Figures S28–S30 of the Supporting Information.

Figure 6 shows representative NMR spectra and kinetics of the most important reactions (for additional spectra, see Supplementary Figures S25 and S26), and Table 3 lists key rate constants, including values determined earlier in magnesium-containing condensation buffer (35). In order to avoid a pH shift that complicates the kinetic picture, we used MOPS buffer in the assays. Control experiments confirmed that the MOPS buffer does not have a significant effect on consumption of EDC (Supplementary Figure S24, Supplementary Information). In the presence of Mg^{2+} cations, we had previously found the isourea EDC-AMP to be all but undetectable by NMR. This changed in magnesium-free medium. Here, a very significant peak ap-

peared for this reactive species (Figure 6A). Further, while in conventional condensation buffer EI-AMP remained a low-level species, EI-AMP made up a significant fraction of the nucleotide species in the Mg^{2+}-free case after 12 h (Figure 6B). Plots of the kinetics for the magnesium-containing and magnesium-free assays show the same phenomenon (Figure 6C, D). In the activation mixture devoid of divalent cations, the active imidazolium nucleotide builds up to a high stationary concentration, rivaling that of AMP after 24 h, whereas with $MgCl_2$ it does not. That the activation reaction is favored in the absence of divalent cations was also apparent from the rate of consumption of EDC, which is high in assays without $MgCl_2$ (see e.g. Supplementary Figure S24b in the Supplementary Information).

Supplementary Table S1 in the Supporting Information lists 13 rate constants for all reaction steps of the network analyzed (compare also Supplementary Figure S27). Supplementary Figure S31 shows chemical fluxes through the reaction channels leading to isourea formation, capture of the isourea to give the imidazolium phosphate EI-AMP, and coupling of this organocapture product with the 2′,3′-diol of another ribonucleotide to give a phosphodiester. The efficient formation and kinetic stability of EI-AMP provides the molecular basis for successful strand formation despite the lack of magnesium ion catalysis. This data further highlights the important roles small heterocycle organocatalysts like 1-ethylimidazole can play in prebiotic processes (35), substituting, in a primitive way, for enzymes or ribozymes that are much harder to form spontaneously from simple precursors.

DISCUSSION

Based on the prevalence of magnesium ions in polymerase active sites and in the assay solutions used for previous oligomerization assays, we assumed that removing the magnesium ions should lower the yields decisively. This was found not to be the case. The yields drop only slightly (C/G/U) or increase (A) when the divalent cation is left out (Table 1). Figure 7 highlights our hypotheses on why this is. Complexation of the phosphate of nucleotides with Mg^{2+} ions lowers their reactivity toward the electrophilic condensation agent. The complexation is expected to be strongest for the most nucleophilic, doubly deprotonated form, which is the kinetically relevant species for the formation of the isourea. This is shown in Figure 7A for the reaction with EDC, but phosphodiester formation in the presence of EI (and a lack thereof in the absence of the organocatalyst) was also shown for cyanamide as condensation agent (see Section 7.2 in the Supporting Information of (35)). The imidazolium phosphate formed upon capturing the isourea with EI is a zwitterion that does not require a counterion. It is apparently sufficiently reactive toward ribose diols by itself, without the need for activation by a divalent cation.

Figure 7B shows a possible molecular scenario for two alternative nucleophilic attacks of the ribose of nucleotides on the activated form EI-AMP. Unlike templated reactions, where preorientation of the nucleophilic alcohol group at the primer terminus and of the electrophilic phosphate of the NTP pre-positions the two reaction partners, the attack in solution may occur via number of different trajectories, particularly when the attack occurs on a free zwitterion rather than a magnesium chelate. The preorienting effects based on confinement and coordination to phosphates that cause the regioselectivity of oligomerizations on clay minerals (21) should be absent. Unencumbered by chelation and preorientation, steric and stereoelectronic factors can thus dominate the regioselectivity. Sterically, a hydroxy group in a pseudo-equatorial position should be more reactive than a hydroxy group in an axial position. In the 3′-endo conformation (North conformation), this is the 3′-hydroxy group, and in the 2′-endo conformation (South conformation), this is the 2′-hydroxy group. Crystal structures of either of the conformations of AMP are known (49,50).

Since the zwitterionic imidazolium species is not coordinated to a magnesium ion, it does not suffer hydrolysis through metal ion catalysis via the release of hydroxide anions from the coordination sphere of the Mg^{2+}, and the hydrolysis of this active form slows down. A similar effect may operate for the isourea, as the dimethylaminopropyl side chain should be mostly in the protonated form at neutral or slightly basic pH. As a consequence, the active forms are longer lived and reach much higher concentrations (Figure 6). This effect apparently overcompensates the lower coupling reactivity in the absence of the magnesium ions. Thus, the overall yield can remain high or even increase when the Lewis acid Mg^{2+} is absent. Further, the unfavorable selectivity toward the 2′,5′-diester gives way to a more balanced reactivity, with 3′,5′-esters as significant or even major isomer. Thus, the 3′,5′-diesters of biological RNA strands can become the main linkage in favorable cases (AMP and basic pH).

CONCLUSIONS

In conclusion, we show that NMR, a high resolution technique suitable for *in situ* monitoring, can provide a wealth of structural information on the products of phosphodiester-forming reactions of nucleotides. Using this technique, untemplated oligomerization of ribonucleotides under magnesium-free conditions were found to give yields and product distributions that are more favorable than previously found in heterogeneous mixtures. The high reactivity and more favorable regioselectivity can be explained based on the properties of the activated species formed *in situ*. Intermediates like EI-NMPs may form from different initial adducts, so that this reaction scheme does not require a specific activating agent, probably making the pathway robust toward changes in what 'chemical fuel' drives condensation reactions in a prebiotic setting.

The magnesium-free oligomerization described here thus provides solutions to several problems of prebiotic chemistry. If significant concentrations of magnesium ions are not required for RNA strands to form, a geochemical constraint is loosened. Further, the lability of RNA toward hydrolysis is much reduced in the absence of Mg^{2+}, so that the products of oligomerization can survive longer. Additionally, the incompatibility of membrane formation based on carboxylic acids or some phospholipids with divalent cations like Mg^{2+} is reduced. Perhaps most importantly, there is no need for clay minerals, and the regioselectivity of phosphodiester formation tilts more toward the natu-

ral 3′,5′-linkages than in the scenarios previously studied. Last, but not least, the efficient mechanistic pathway via zwitterionic organocatalytic intermediates avoids artificial preactivation steps and provides an avenue to regulation by changing the concentration of small, nucleobase-like heterocycles, without the need for enzymes as catalysts in a molecular world devoid of encoded biomacromolecules.

SUPPLEMENTARY DATA

Supplementary Data are available at NAR Online.

ACKNOWLEDGEMENTS

The authors thank Prof. U.E. Steiner for help with kinetics, Dr B. Claasen for assistance with NMR spectra, and M. Räuchle for sharing results on peptido RNA synthesis.

FUNDING

Deutsche Forschungsgemeinschaft [RI 1063/16-1, CRC TRR 235, project P06 to C.R.]. Funding for open access charge: University of Stuttgart.
Conflict of interest statement. None declared.

REFERENCES

1. Gesteland,R.F., Cech,T.R. and Atkins,J.F. (1999) *The RNA World*. 2nd edn. Cold Spring Harbor Press, NY.
2. Ruiz-Mirazo,K., Briones,C. and de la Escosura,A. (2014) Prebiotic systems chemistry: new perspectives for the origins of life. *Chem. Rev.*, **114**, 285–366.
3. Orgel,L.E. (2004) Prebiotic chemistry and the origin of the RNA world. *Crit. Rev. Biochem. Mol. Biol.* **39**, 99–123.
4. Neveu,M., Kim,H. and Benner,S.A. (2013) The “strong” RNA world hypothesis: fifty years old. *Astrobiology*, **13**, 391–403.
5. Higgs,P.G. and Lehman,N. (2015) The RNA world: molecular cooperation at the origins of life. *Nat. Rev. Gen*, **16**, 7–17.
6. Powner,M.W., Sutherland,J.D. and Szostak,J.W. (2010) Chemoselective multicomponent one-pot assembly of purine precursors in water. *J. Am. Chem. Soc.*, **132**, 16677–16688.
7. Becker,S., Thoma,I., Deutsch,A., Gehrke,T., Mayer,P., Zipse,H. and Carell,T. (2016) A high-yielding, strictly regioselective prebiotic purine nucleoside formation pathway. *Science*, **352**, 833–836.
8. Kozlov,I.A. and Orgel,L.E. (2000) Nonenzymatic template-directed synthesis of RNA from monomers. *Mol. Biol.*, **34**, 781–789.
9. Moravek,J. (1967) Formation of oligonucleotides during heating of a mixture of uridine 2′(3′)-phosphate and uridine. *Tetrahedron Lett.*, **18**, 1707–1710.
10. Beckmann,C., Kirby,A.J., Kuusela,S. and Tickle,D.C. (1998) Mechanisms of catalysis by imidazole buffers of the hydrolysis and isomerisation of RNA models. *J. Chem. Soc. Perkin Trans.*, **2**, 573–581.
11. Wasner,M., Arion,D., Borkow,G., Noronha,A., Uddin,A.H., Parniak,M.A. and Damha,M.J. (1998) Physicochemical and biochemical properties of 2′-5′-linked RNA and 2′-5′-RNA:3′-5′-RNA “hybrid” duplexes. *Biochemistry*, **37**, 7487–7486.
12. Engelhart,A.E., Powner,M.W. and Szostak,J.W. (2013) Functional RNAs exhibit tolerance for non-heritable 2′-5′versus 3′-5′ backbone heterogeneity. *Nat. Chem.*, **5**, 390–394.
13. Prakash,T.P., Roberts,C. and Switzer,C. (1997) Activity of 2′,5′-linked RNA in the template-directed oligomerization of mononucleotides. *Angew. Chem. Int. Ed. Engl.*, **36**, 1522–1523.
14. Usher,D.A. and McHale,A.H. (1976) Hydrolytic stability of helical RNA: A selective advantage for the natural 3′,5′- bond. *Proc. Natl. Acad. Sci. U.S.A.*, **73**, 1149–1153.
15. Szostak,J.W. (2012) The eightfold path to non-enzymatic RNA replication. *J. Syst. Chem.*, **3**, 2.
16. Cafferty,B.J. and Hud,N.V. (2014) Abiotic synthesis of RNA in water: a common goal of prebiotic chemistry and bottom-up synthetic biology. *Curr. Opin. Chem. Biol.*, **22**, 146–157.
17. Sulston,J., Lohrmann,R., Orgel,L.E. and Miles,H.T. (1968) Nonenzymatic synthesis of oligoadenylates on a polyuridylic acid template. *Prod. Natl. Acad. Sci. U.S.A.*, **59**, 726–733.
18. Sawai,H. (1976) Catalysis of internucleotide bond formation by divalent metal ions. *J. Am. Chem. Soc.*, **98**, 7037–7039.
19. Orgel,L.E. and Lohrmann,R. (1978) Preferential formation of (2′-5′)-linked internucleotide bonds in non-enzymatic reactions. *Tetrahedron Lett.*, **34**, 853–855.
20. Joshi,P.C., Aldersley,M.F., Delano,J.W. and Ferris,J.P. (2009) Mechanism of montmorillonite catalysis in the formation of RNA oligomers. *J. Am. Chem. Soc.*, **131**, 13369–13374.
21. Ferris,J.P. and Ertem,G. (1992) Oligomerization of ribonucleotides on montmorillonite: Reaction of the 5′-phosphorimidazolide of adenosine. *Science*, **257**, 1387–1389.
22. Prahabar,K.J., Cole,T.D. and Ferris,J.P. (1994) Effect of phosphate activating group on oligonucleotide formation on montmorillonite: the regioselective formation of 3′,5′-linked oligoadenylates. *J. Am. Chem. Soc.*, **116**, 10914–10920.
23. Prabahar,K.J. and Ferris,J.P. (1997) Adenine derivatives as phosphate-activating groups for the regioselective formation of 3′,5′-linked oligoadenylates on montmorillonite: Possible phosphate-activating groups for the prebiotic synthesis of RNA. *J. Am. Chem. Soc.*, **119**, 4330–4337.
24. Miyakawa,S. and Ferris,J.P. (2003) Sequence- and regioselectivity in the montmorillonite-catalyzed synthesis of RNA. *J. Am. Chem. Soc.*, **125**, 8202–8208.
25. Verlander,M.S., Lohrmann,R. and Orgel,L.E. (1973) Catalysts for the self-polymerization of adenosine cyclic 2′, 3′-phosphate. *J. Mol. Evol.*, **2**, 303–316.
26. Kanavarioti,A., Monnard,P.-A. and Deamer,D.W. (2001) Eutectic phases in ice facilitate nonenzymatic nucleic acid synthesis. *Astrobiology*, **1**, 271–281.
27. Ferris,J.P. and Ertem,G. (1992) Oligomerization reactions of ribonucleotuides: the reaction of the 5′-phosphorimidazolide of nucleosides on montmorillonite and other minerals. *Origins Life Evol. Biosphere*, **22**, 369–381.
28. Jheeta,S. and Joshi,.P.C. (2014) Prebiotic RNA synthesis by montmorillonite catalysis. *Life*, **4** 318–330.
29. Kawamura,K. and Ferris,J.P. (1994) Kinetic and mechanistic analysis of dinucleotide and oligonucleotide formation from the 5′-phosphorimidazolide of adenosine on Na+-montmorillonite. *J. Am. Chem. Soc.* **116**, 7564–7572.
30. Sgrignani,J. and Magistrato,A. (2012) The structural role of Mg2+ Ions in a class I RNA polymerase ribozyme. *J. Phys. Chem. B*,**116**, 2259−2268.
31. Athavale,S.S., Petrov,A.S., Hsiao,C., Watkins,D., Prickett,C.D., Lie,L., Bowman,J.C., O’Neill,E., Bernier,C.R. *et al.* (2012) RNA folding and catalysis mediated by iron (II). *PLoS One*, **7**, e38024.
32. Wochner,A., Attwater,J., Coulson,A. and Holliger,P. (2011) Ribozyme-catalyzed transcription of an active ribozyme. *Science*, **332**, 209–212.
33. Westover,K.D., Bushnell,D.A. and Kornberg,R.D. (2004) Structural basis of transcription: nucleotide selection by rotation in the RNA polymerase II active center. *Cell*, **119**, 481–489.
34. Jauker,M., Griesser,H. and Richert,C. (2015) Copying of RNA sequence without pre-activation. *Angew. Chem. Int. Ed.*, **54**, 14559–14563.
35. Tremmel,P., Griesser,H., Steiner,U.E. and Richert,C. (2019) How small heterocycles make a reaction network of amino acids and nucleotides efficient in water. *Angew. Chem. Int. Ed.*, **58**, 13087–13092.
36. Richert,C. (2018) Prebiotic chemistry and human intervention. *Nat. Commun.*, **9**, 5177.
37. Benner,S.A., Bell,E.A., Biondi,E., Brasser,R., Carell,T., Kim,H., Mojzsis,S.J., Omran,A., Pasek,M.A. and Trail,D. (2019) When did life likely emerge on earth in an RNA-first process? *Chem. Syst. Chem.*, **1**, e190003.
38. Kanavarioti,A., Bernasconi,C.F. and Baird,E. (1998) Effects of monomer and template concentration on the kinetics of nonenzymatic template-directed oligoguanylate synthesis. *J. Am. Chem. Soc.*, **120**, 8575–8580.

39. Horn,T. and Urdea,M.S. (1986) A chemical 5'-phosphorylation of oligodeoxyribonucleotides that can be monitored by trityl cation release. *Tetrahedron Lett.*, **27**, 4705–4708.
40. Jauker,M., Griesser,H. and Richert,C. (2015) Spontaneous formation of RNA strands, peptidyl RNA, and cofactors. *Angew. Chem. Int. Ed.*, **54**, 14564–14569.
41. Griesser,H., Bechthold,M., Tremmel,P., Kervio,E. and Richert,C. (2017) Amino acid-specific, ribonucleotide-promoted peptide formation in the absence of enzymes. *Angew. Chem. Int. Ed.*, **56**, 1224–1228.
42. Griesser,H., Tremmel,P., Kervio,E., Pfeffer,C., Steiner,U.E. and Richert,C. (2017) Ribonucleotides and RNA promote peptide chain growth. *Angew. Chem. Int. Ed.*, **56**, 1219–1223.
43. Gite,S.U. and Shankar,V. (1995) Single-strand-specific nucleases. *Crit. Rev. Microbiol.*, **21**, 101–122.
44. Kondo,N.S., Holmes,H.M., Stempel,L.M. and Ts'o,P.O. (1970) Influence of the phosphodiester linkage (3′-5′, 2′-5′ and 5′-5′) on the conformation of dinucleoside monophosphate. *Biochemistry*, **9**, 3479–3498.
45. Ezra,F.S., Kondo,N.S., Ainsworth,C.F. and Danyluk,S.S. (1976) The effect of (2′-5′) and (3′-5′) phosphodiester linkages on conformational and stacking properties of cytidyl-cytidine in aqueous solution. *Nucleic Acids Res.*, **3**, 2549–2562.
46. Imai,J. and Torrence,P.F. (1985) Expedient chemical synthesis of sequence-specific 2′,5′-oligonucleotides. *J. Org. Chem.*, **50**, 1418–1426.
47. Torrence,P.F., Imai,J., Lesiak,K., Jamoulle,J-C. and Sawai,H. (1984) Oligonucleotide structural parameters that influence binding of 5′-O-Triphosphoadenyl-(2′,5′)′-adenyl-(2′,5′)-adenosine to the 5′-O-Triphosphoadenyl-(2′,5′)′-adenyl-(2′,5′)-adenosine dependent endoribonuclease: chain length, phosphorylation state, and heterocycle base. *J. Med. Chem.*, **27**, 726–733.
48. Gopalakrishnan,V., Ganesh,K.N., Gunjal,A. and Likhite,S.M. (1991) Spectroscopic and enzymatic characterization of 2′-5′-and 3′-5′-RNA hexamers AACCUU synthesized by phosphotriester approach in solution using 2′-t-butyldimethylsilyl protection. *Tetrahedron*, **47**, 1075–1090.
49. Kraut,J. and Jensen,L.H. (1963) Refinement of the crystal structure of adenosine-5′-phosphate. *Acta Cryst.*, **16**, 79–88.
50. Neidle,S., Kühlbrandt,W. and Achari,A. (1976) The crystal structure of an orthorhombic form of adenosine-5′-monophosphate. *Acta Cryst.*, **32**, 1850–1855.